Risk-Adjusted Strategies to Protect Food Supply and Farmer Livelihoods in West Africa – Supplementary Information

Debbora Leip[1,2], Elena Rovenskaya[1,3], and Matthias Wildemeersch[1]

[1]International Institute for Applied Systems Analysis (IIASA), Austria
[2]Potsdam Institute for Climate Impact Research (PIK), Germany
[3]Faculty of Computational Mathematics and Cybernetics, Lomonosov Moscow State University, Russia

1 Determining the optimal number of clusters

The k-medoids clustering algorithm can be performed for any given number of clusters k, but we aim to find the number of clusters that maximizes the intra-cluster similarity, while minimizing the inter-cluster similarity. Intra-cluster similarity is defined as the average Pearson distance between the SPEI time series of any cell and its respective medoid, while the inter-cluster similarity is defined as the average Pearson distance between any medoid and its closest neighbor. While for an increasing number of clusters the average distance within clusters will tend towards zero, the average distance between clusters will never reach one under realistic conditions using the Pearson distance, as medoids would have to be perfectly anti-correlated. We therefore use the maximal observed average distance between medoids as reference distance, in this case 0.62, obtained for $k = 2$. Different numbers of clusters are subsequently ranked based on the Euclidean distance between the points in the scatter plot of intra-and inter-cluster distances and the utopian point (0, 0.62), as depicted in Fig. 1. The optimal number of clusters is thus defined as 9. Note that the residual yield correlation between the nine regions is ignored in the stochastic modelling framework, implying that reported benefits of cooperation represent an upper performance bound.

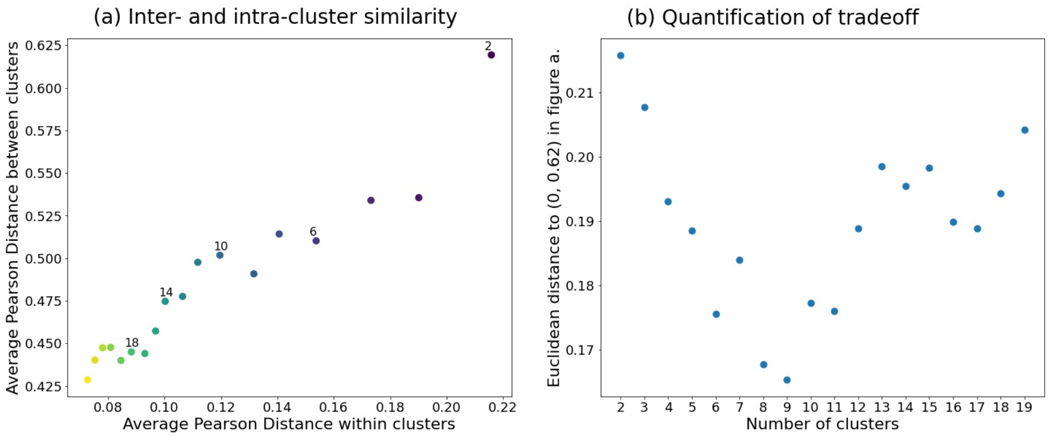

Figure 1: **(a)** Inter- and intra-cluster similarity. A trade-off can be observed between high similarity within a cluster and high dissimilarity between clusters. The utopian point is situated in the top left corner of the graph. **(b)** Optimal trade-off between inter- and intra-cluster similarity. The Euclidean distance with respect to the utopian point is depicted as a function of the number of clusters. The minimum Euclidean distance is achieved for nine clusters.

2 Crop yield projections for the nine established regions

Crop yield projections are based on a linear regression model for maize and rice in the nine considered regions. The time series of the expected yields of both crops in each region, together with the corresponding linear regressions are depicted in Fig. 2. Expected yield projections over the time horizon of interest, together with the uncertainty around the trends is depicted in Fig. 3. The yield distributions for both crops in each region are further depicted in Fig. 4 and Fig. 5 for the years 2016 and 2030, respectively.

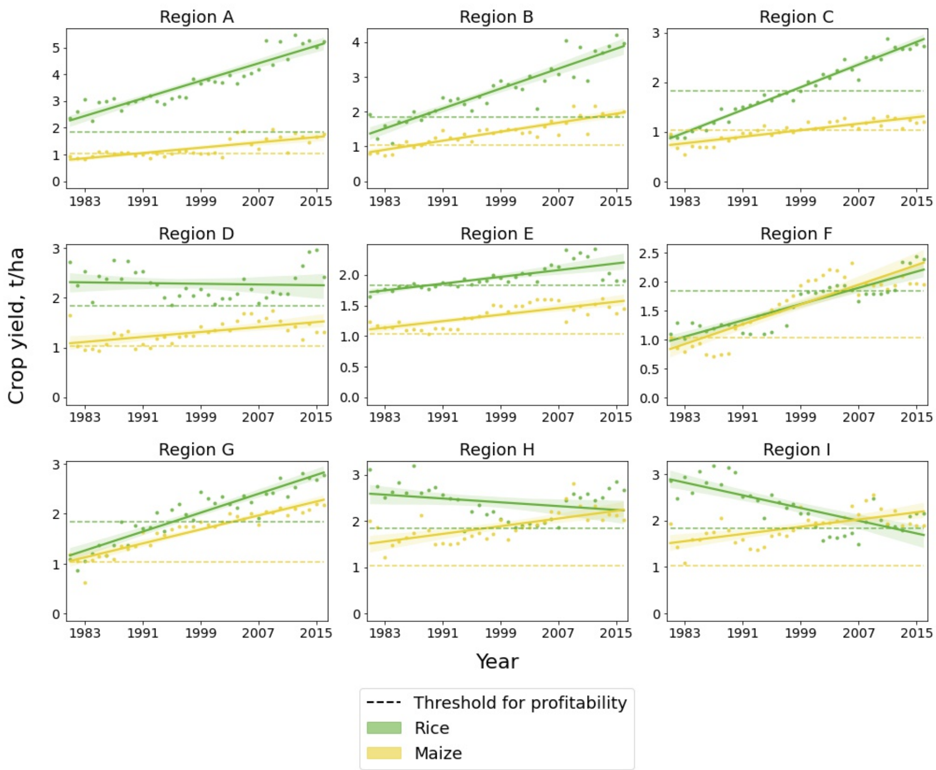

Figure 2: **Linear regression model.** The trends of expected yields in the nine considered regions show different patterns. In 2016, the yield of rice is higher than the yield of maize in six of the nine regions, and crop yield differences can be substantial, i.e., higher than a factor 2. The shaded area represents the 95% confidence interval of the linear regression.

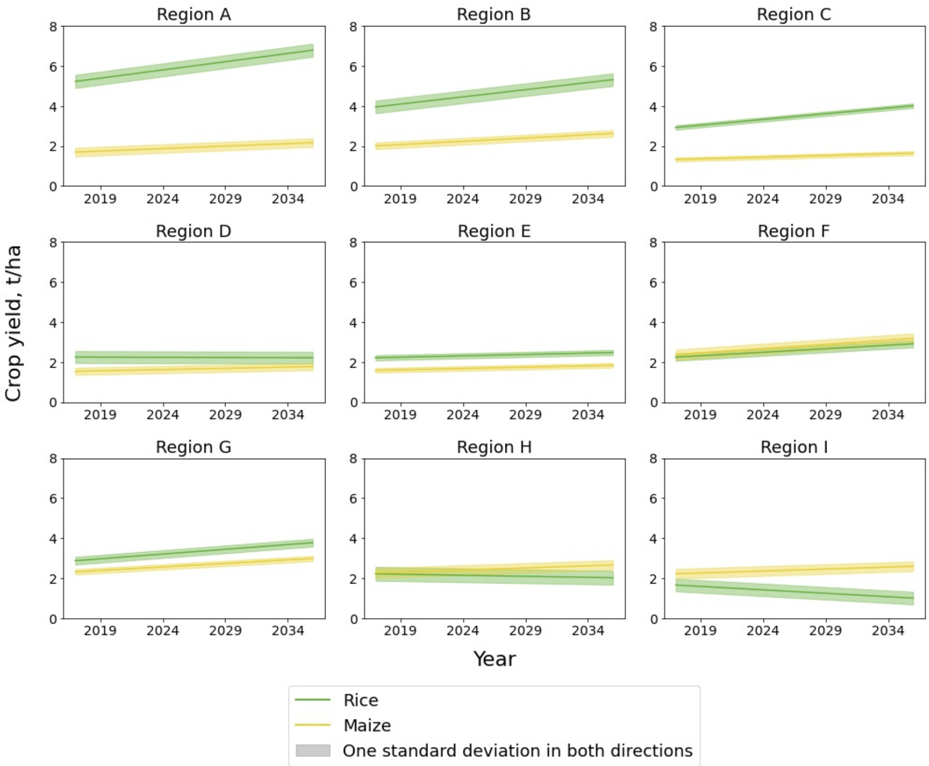

Figure 3: Yield projections over time horizon of interest using the linear regression model. The shaded area represents one standard deviation.

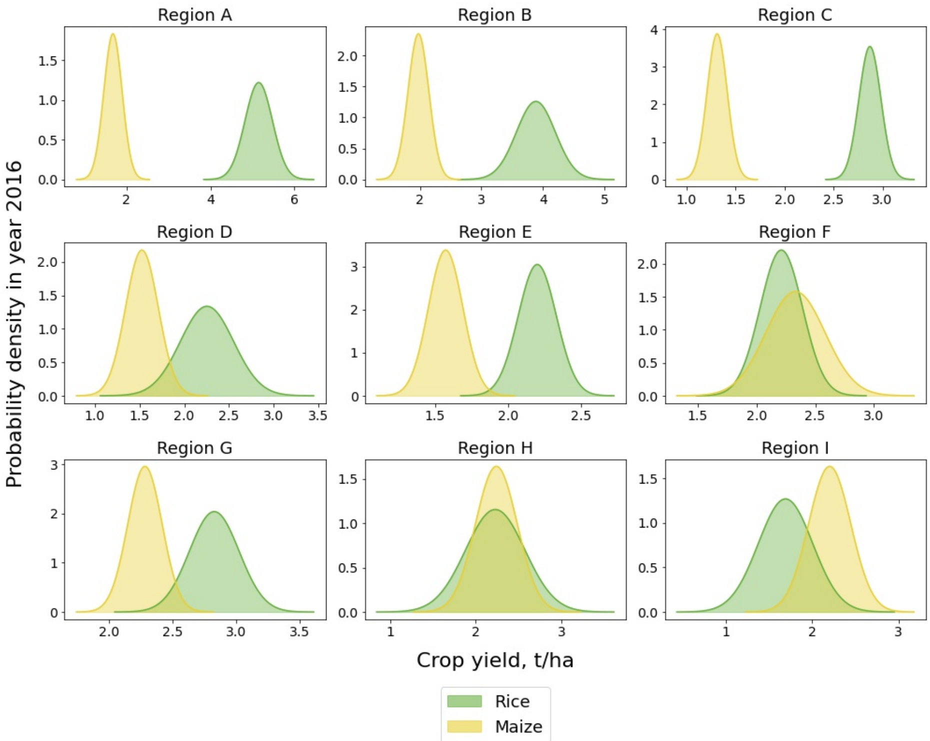

Figure 4: **Modelled crop yield distributions for the year 2016.** Modelled crop yields for rice and maize show large diversity in terms of expected yield and yield variance in the nine regions. In six of the nine regions, the expected crop yield is higher for rice than for maize, although rice is also subject to higher crop yield variations.

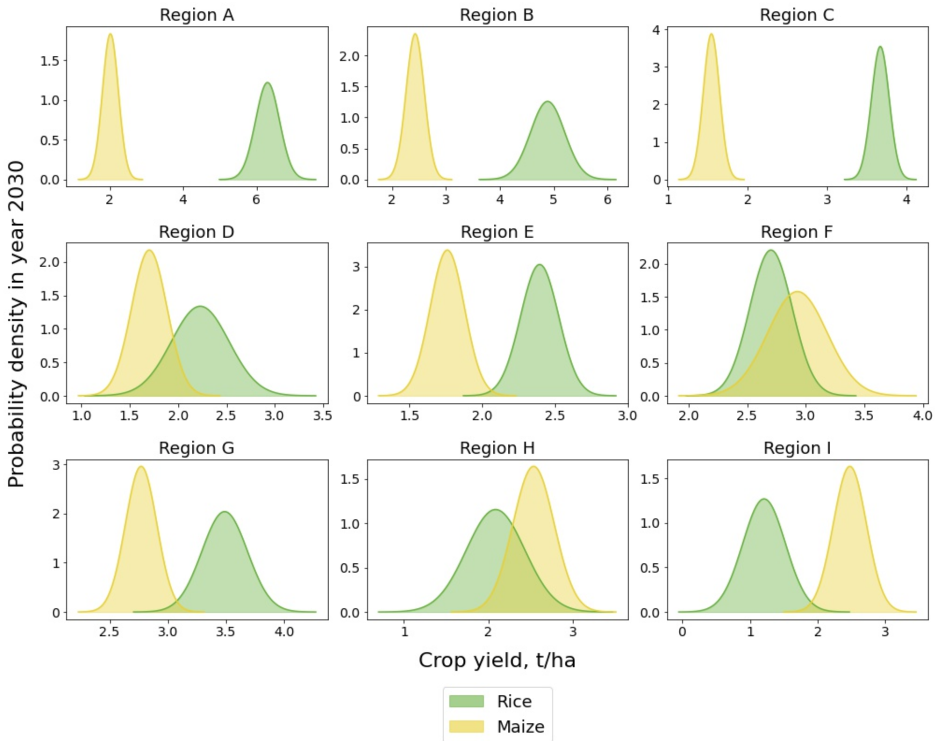

Figure 5: **Modelled crop yield distributions for the year 2030.** Modelled crop yields follow a trend-stationary process, i.e., crop yields are stationary around a linear trend. Due to the crop yield trends, we observe larger differences in expected crop yields in 2030 than in 2016.

3 Model parameters

To determine the average farm gate price for rice and maize in West Africa, we use FAO time series for producer prices per ton and for each country [1]. For each crop we take the average of the farm gate prices per country over the FAO time series (see Fig. 6), and then calculate a weighted average p_j of the resulting country values with weights given by the share of each country in the total considered area in West Africa. This results in a single farm gate price for rice and maize each, which we assume to be constant over the considered time window (Table 1). Cultivation costs c_j [$/ha] are based on per hectare costs for each crop, and are also assumed constant over the regions and over time. We calculate an average value over different case studies (Table 1): for rice, we rely on studies on Liberia [2], Kaduna State in Nigeria [3], and Benin, Burkina-Faso, Mali, and Senegal [4]; for maize, the case studies cover Niger State in Nigeria [5], and Benin, Ghana, and Cote d'Ivoire [6].

Notation	Description	Value	Source
p_{rice}	farm gate price rice	343.82 $/t	[1]
p_{maize}	farm gate price maize	266.30 $/t	[1]
c_{rice}	cultivation cost for rice	643.44 $/ha	[2, 3, 4]
c_{maize}	cultivation cost for maize	281.22 $/ha	[5, 6]
a_{rice}	calorie content of rice	3.6 10^6 kcal/t	[7]
a_{maize}	calorie content of maize	3.65 10^6 kcal/t	[7]

Table 1: Model parameters.

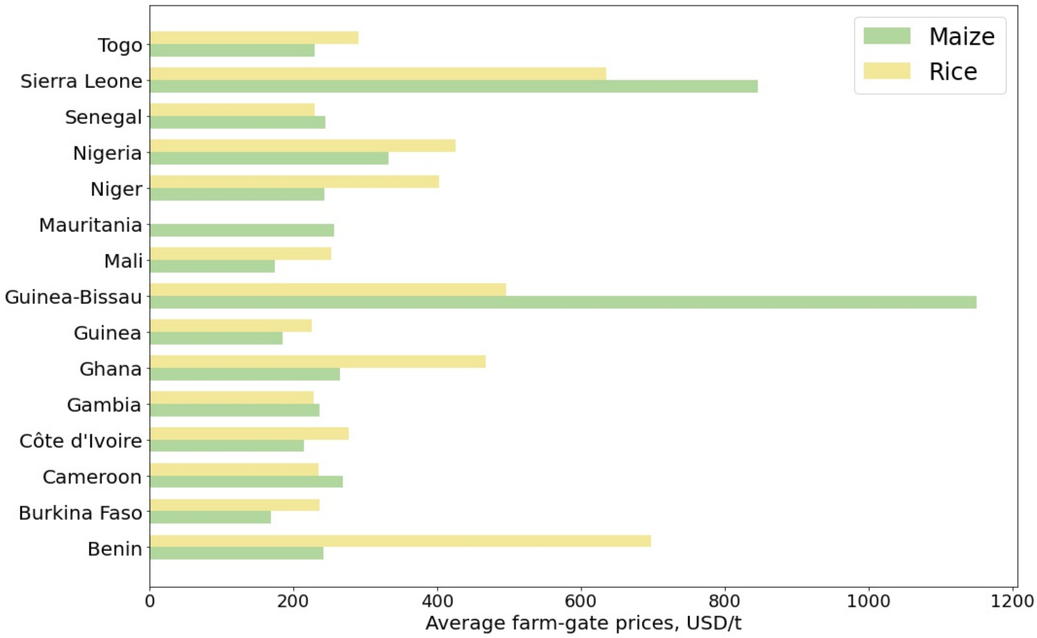

Figure 6: Average farm gate prices [USD/t] for maize and rice in different West African countries.

4 Linearization of the optimization framework

Since the expectations in (6) and (7) of the Methods Section in the main manuscript cannot be solved analytically in general, we approximate the expected value with the sample mean and get

$$\begin{aligned}
\min_{x} \quad & \frac{1}{\mathcal{N}} \sum_{n=1}^{\mathcal{N}} \Bigg[\sum_{t=t_0}^{T_{\text{fin}}(m^n)} \sum_{k \in \mathcal{P}_i} \sum_{j=1}^{\mathcal{J}} x_{j,k,t} \cdot c_{j,k} \\
& + \sum_{t=t_0}^{T_{\text{fin}}(m^n)} \Bigg(\rho \cdot \max \Big\{ 0,\, d_t - \sum_{k \in \mathcal{P}_i} \sum_{j=1}^{\mathcal{J}} y^n_{j,k,t} \cdot x_{j,k,t} \cdot a_j \Big\} \Bigg) \Bigg] \\
\text{s.t.} \quad & x_{j,k,t} \geq 0 && \forall\, j, t\, ; \forall\, k \in \mathcal{P}_i \\
& \sum_{j=1}^{\mathcal{J}} x_{j,k,t} \leq \bar{x}_k && \forall\, t\, ; \forall\, k \in \mathcal{P}_i .
\end{aligned} \tag{S1}$$

The objective function in (S1) is non-smooth due to the max-operator, and we can linearize the optimization problem by using the epigraph form of (S1) [8]. Using this approach, the optimization problem can be written as follows

$$\begin{aligned}
\min_{x, v_{t,n}} \quad & \frac{1}{\mathcal{N}} \sum_{n=1}^{\mathcal{N}} \Bigg[\sum_{t=t_0}^{T_{\text{fin}}(m^n)} \sum_{k \in \mathcal{P}_i} \sum_{j=1}^{\mathcal{J}} x_{j,k,t} \cdot c_{j,k} + \rho \sum_{t=t_0}^{T_{\text{fin}}(m^n)} v_{t,n} \Bigg] \\
\text{s.t.} \quad & x_{j,k,t} \geq 0 && \forall j, t; \forall\, k \in \mathcal{P}_i \\
& \sum_{j=1}^{\mathcal{J}} x_{j,k,t} \leq \bar{x}_k && \forall t; \forall\, k \in \mathcal{P}_i \\
& v_{t,n} \geq 0 && \forall t, n \\
& v_{t,n} \geq \Big(d_t - \sum_{k \in \mathcal{P}_i} \sum_{j=1}^{\mathcal{J}} y^n_{j,k,t} \cdot x_{j,k,t} \cdot a_j\Big) && \forall t, n
\end{aligned} \tag{S2}$$

This problem is fully linearized and can be efficiently solved using standard solvers in Python.

Note in (1) of the main manuscript that in the rare cases of negative profits, the regions perform a tax refund to the farmers, which is common in different tax systems. Although the tax refund can be removed from the model formulation, this allows the model to remain linear and has substantial benefits for the numerical complexity of the stochastic program without big implications for the model realism. Similarly, the payouts to farmers could by capped by I_k^{gov}, i.e., not covering a part of the actual loses farmers may have. For reasons of computational efficiency we decide not to do so without substantial implications for the realism of the model.

5 Food production under the risk-neutral and risk-target strategy

Food production distributions are depicted in Fig. 7 and illustrate how the food production changes as the reliability target for food production increases. In seven of the nine regions, the production is increased as the reliability target gets higher. However, in regions H and I, all land is already allocated in the risk-neutral strategy and therefore, increasing the reliability target for food production does not affect production.

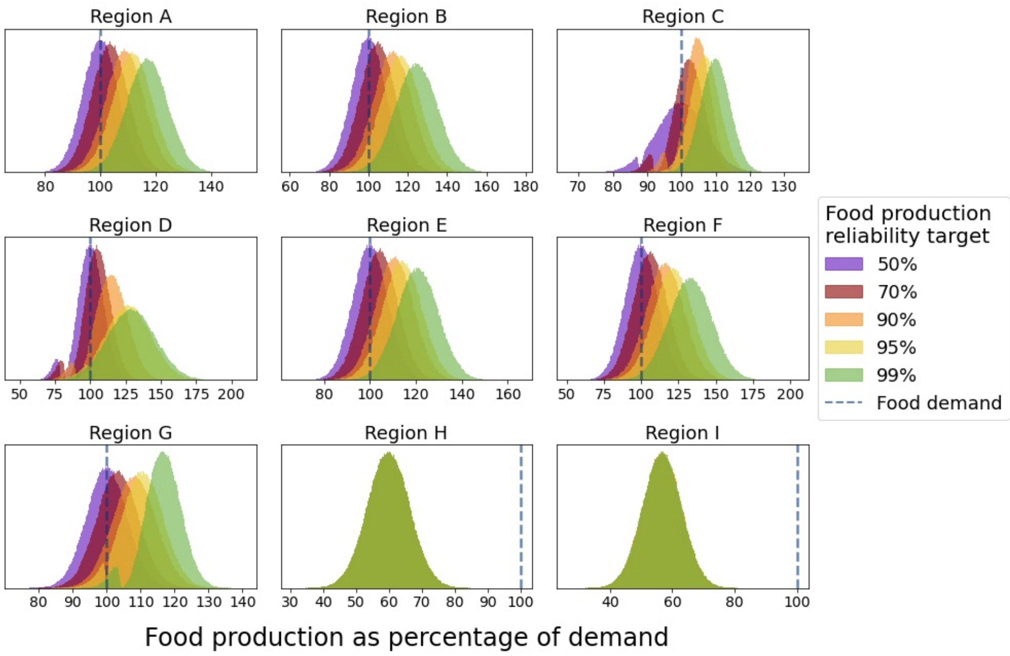

Figure 7: **Food production distributions in West Africa.** The distributions correspond to different reliability targets under the risk-neutral and risk-target strategy, and apply to the stationary development scenario.

The expected food shortage at the West African scale is depicted as a function of the reliability target for food production in Fig. 8. Most of the individual regions substantially reduce the expected food shortage by applying higher reliability targets for food production. However, region H and I suffer a considerable food shortage even if all available arable land is used in the risk-neutral strategy. The bad performance of the highly populated regions H and I in Nigeria results in a moderate reduction of expected food shortages at the West African scale, since increasing the reliability target for food production is without effect in these regions.

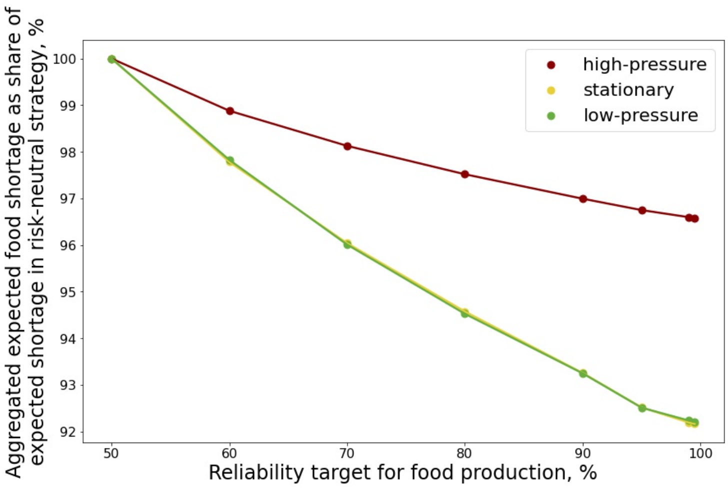

Figure 8: Expected food shortage at the West African scale relative to the expected food shortage of the risk-neutral strategy.

6 Optimal crop allocation in the risk-target strategy

The dynamics of land allocation for rice and maize over the considered time frame and in the nine regions are depicted in Fig. 9 and Fig. 10 for reliability targets equal to 99% and 90%, respectively. The progressive substitution between crops in regions D, E, and G for the 99% reliability target are observable. In region E, no substitution takes place for a lower reliability target of 90%, since enough maize can be produced to reach the reliability target for food production.

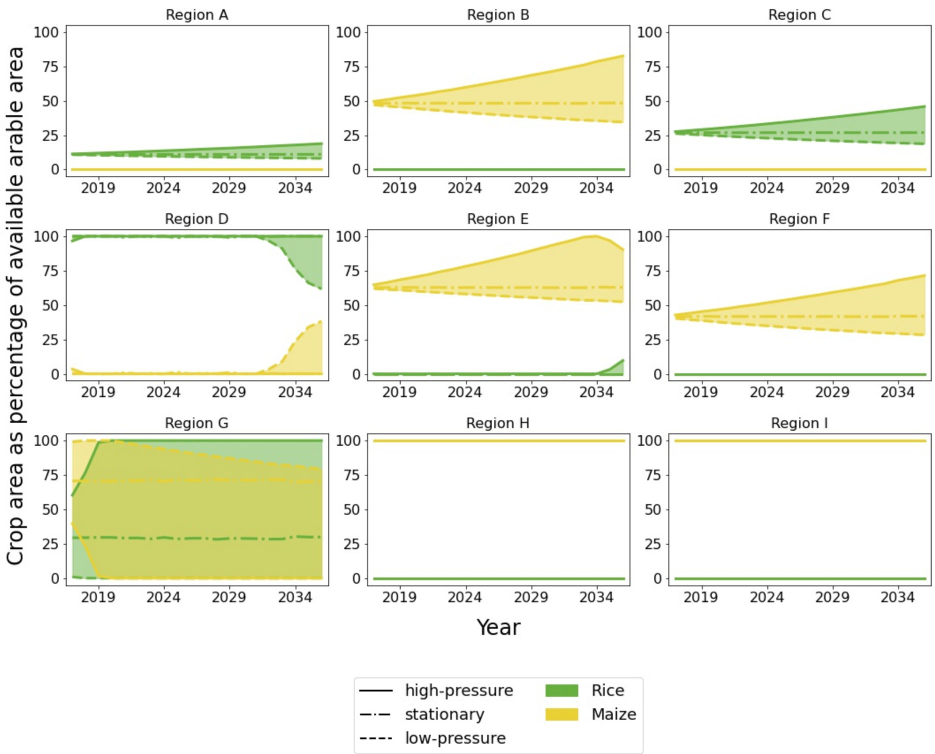

Figure 9: Land allocation over time for a reliability target of 99%

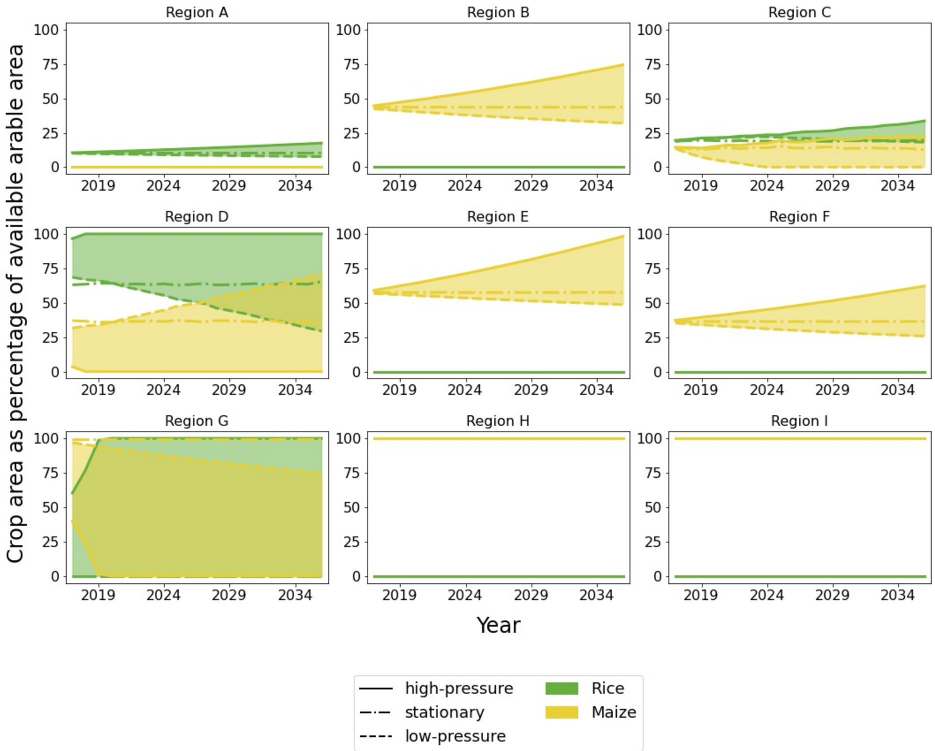

Figure 10: Land allocation over time for a reliability target of 90%.

7 Distributions of farmer profits and fund capital

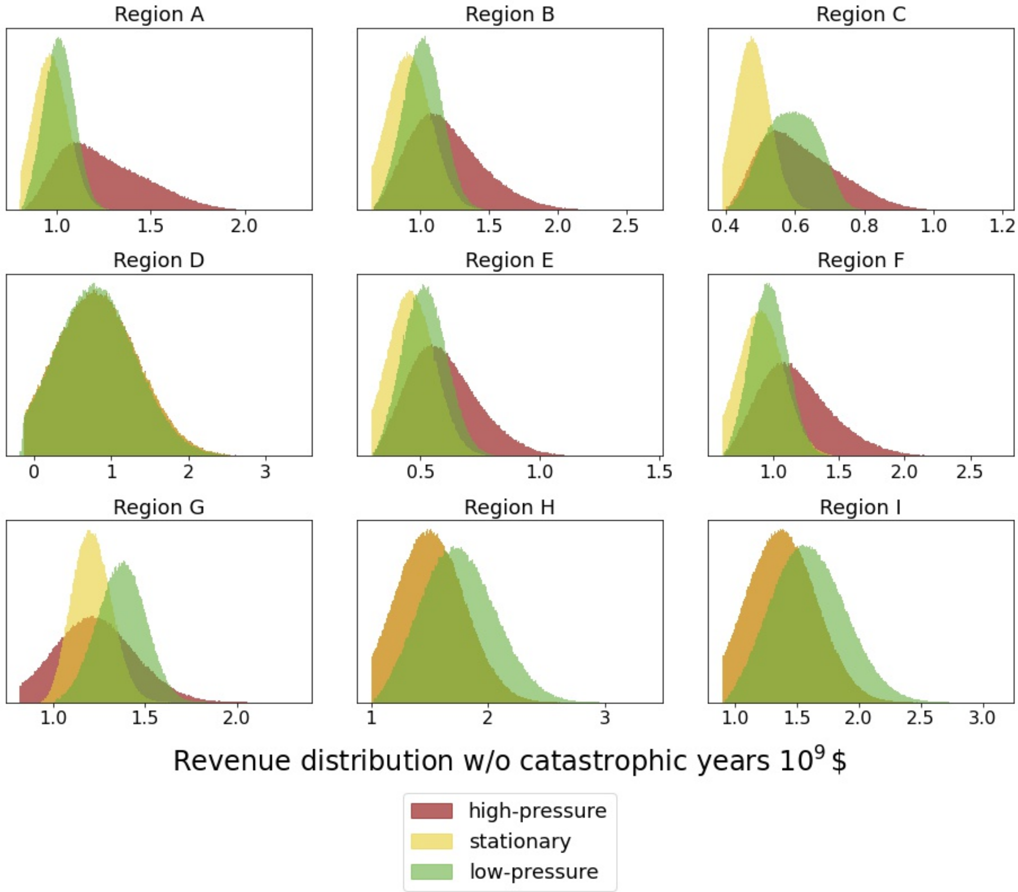

Figure 11: **Farmer profit distribution excluding cases with fund payouts.** The cut-off at the lower tail of the profit distribution indicates the protection of farmer livelihoods. Cases with fund payouts are omitted from the graph, as they result in high peaks corresponding to the guaranteed income. In the high-pressure scenario with growing population, the guaranteed income is scaled according to the population resulting in a wider profit distribution.

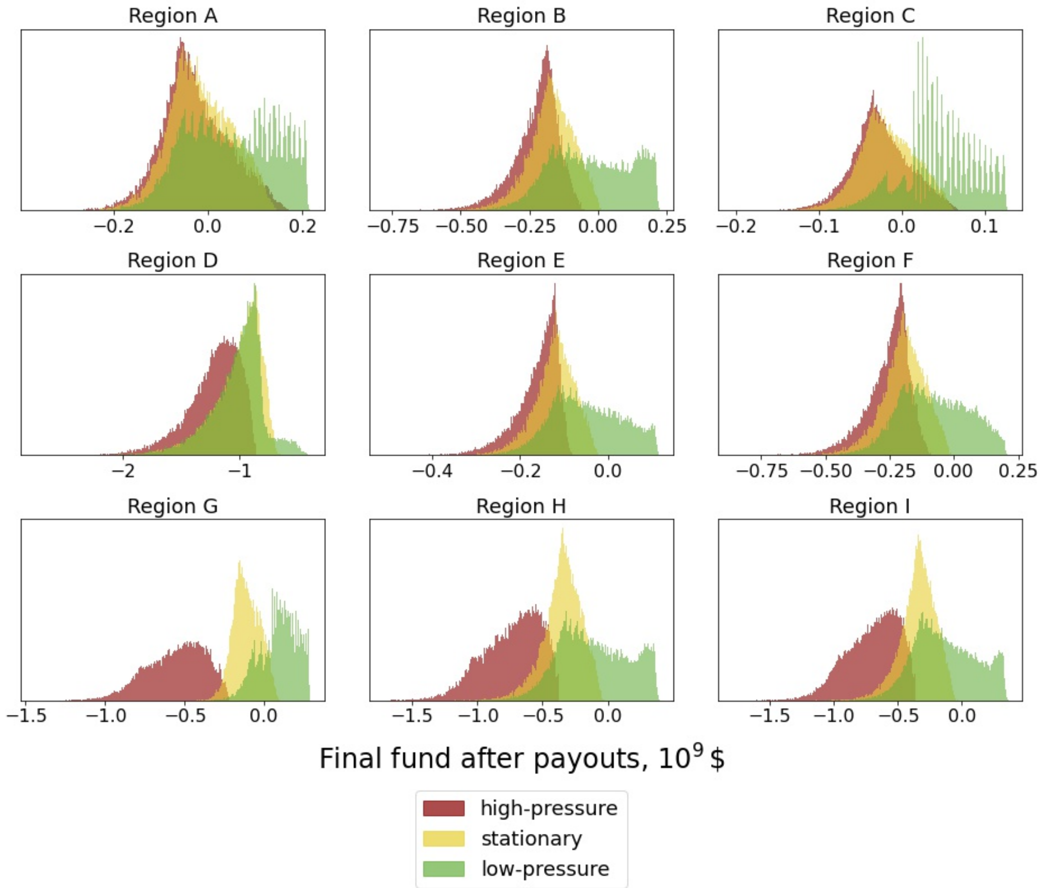

Figure 12: Fund capital distribution after payouts in the event of catastrophic yields.

References

[1] FAOSTAT. Producer prices. https://https://www.fao.org/faostat/en/#data/PP. Accessed: 2022-01-11.

[2] Ministry of Agriculture (Liberia). Liberia: Invest agriculture, 2019. https://ekmsliberia.info/document/liberia-invest-agriculture/. Accessed: 2022-01-11.

[3] G.N. Ben-Chendo, N. Lawal, and M.N. Osuji. Cost and returns of paddy rice production in Kaduna state. *European Journal of Agriculture and forestry Research*, 5(3):41–48, 2017.

[4] Amadou Abdoulaye FALL. Synthèse des études sur l'état des lieux chaine de valeur riz en Afrique de l'ouest: Bénin, Burkina Faso, Mali, Niger et Sénégal. *Rapport final, ROPPA, 83p*, 2016.

[5] M.S. Sadiq, M.T. Yakasai, M.M. Ahmad, T.Y. Lapkene, and Mohammed Abubakar. Profitability and production efficiency of small-scale maize production in Niger State, Nigeria. *IOSR Journal of Applied Physics*, 3(4):19–23, 2013.

[6] Mahamadou Nassirou Ba. Competiveness of maize value chains for smallholders in West Africa: Case of Benin, Ghana and Cote D'Ivoire. *Agricultural Sciences*, 8(12):1372–1401, 2017.

[7] Agricultural Research Service US Department of Agriculture. USDA national nutrient database for standard reference, release 28 (slightly revised). version current: May 2016. https://www.ars.usda.gov/northeast-area/beltsville-md-bhnrc/beltsville-human-nutrition-research-center/methods-and-application-of-food-composition-laboratory/mafcl-site-pages/sr11-sr28/. Accessed: 2022-09-18.

[8] Stephen Boyd and Lieven Vandenberghe. *Convex optimization*. Cambridge university press, 2004.